

A simple and accurate four-node quadrilateral element using stabilized nodal integration for laminated plates

H. Nguyen-Van¹, N. Mai Duy² and T. Tran-Cong³

Abstract: This paper reports the development of a simple but efficient and accurate four-node quadrilateral element for models of laminated, anisotropic plate behaviour within the framework of the first-order shear deformation theory. The approach incorporates the strain smoothing method for mesh-free conforming nodal integration into the conventional finite element techniques. The membrane-bending part of the element stiffness matrix is calculated by the line integral on the boundaries of the smoothing elements while the shear part is performed using an independent interpolation field in the natural co-ordinate system. Numerical results show that the element offered here is locking-free for extremely thin laminates, reliable and accurate, and easy to implement. Its convergence properties are insensitive to mesh distortion, thickness-span ratios, lay-up sequence and degree of anisotropy.

Keyword: laminated composite plates, strain smoothing method, shear-locking free, first-order shear deformation theory.

1 Introduction

Fibre-reinforced composite materials are ideal for many engineering applications that require high strength-to-weight, stiffness-to-weight ratios, excellent resistance to corrosive substances and potentially high overall durability. In recent years, a fast growing interest in the use of fibre-reinforced

composite structures, especially laminated plates and shells in various civil and mechanical engineering applications, is evidenced by numerous efforts to develop the rational analysis of these structures. For example, the research on simple, efficient and accurate modeling of thin to thick composite plates and shells has caught the attention of many practitioners in the field of analysis and design of composite material structures.

There are many theories developed for linear/nonlinear analysis of thin to thick laminated plates in bending such as the classical plate theory (CPT), the first-order shear deformation theory (FSDT), the higher-order shear deformation theory (HSDT), the layer-wise theory and variable kinematics models. Among these theories, the FSDT is often widely used due to its simplicity, low computational cost and the ability of simulating the shear deformation effects in laminated plates and shell structures through appropriate shear correction factors (SCFs). These factors depend on the constituent ply properties, ply lay-up, fibre orientation, boundary conditions and particular applications and can be calculated using some special procedures [Valchoutsis (1992); Chatterjee and Kulkarni (1979); Whitney (1973)]. With the proper SCFs, the use of FSDT becomes more reasonable in practical applications.

To date, FSDT is still the most attractive approach owing to a good compromise between numerical accuracy and computational burden. Many researchers have made significant contributions to the development of simple triangular and quadrilateral elements based on FSDT for many years. The major problem is how to remove shear-locking as the thickness-span ratio of the plate become too small (e.g. $h/a < 1/50$). Many techniques have been proposed

¹ Computational Engineering & Science Research Center (CESRC), Faculty of Engineering & Surveying, USQ, Australia.

² Computational Engineering & Science Research Center (CESRC), Faculty of Engineering & Surveying, USQ, Australia.

³ Computational Engineering & Science Research Center (CESRC), Faculty of Engineering & Surveying, USQ, Australia.

to overcome this phenomenon, with varying degree of success. For instance, the reduced or selective integration methods [Zienkiewicz, Taylor, and Too (1971); Pawsey and Clough (1971); Hughes, Cohen, and Haroun (1978); Pugh, Hinton, and Zienkiewicz (1978); Pugh, Hinton, and Zienkiewicz (1978); Malkus and Hughes (1978)]; the hybrid/mixed method [Hughes and Tezduar (1981); Crisfield (1984); Zienkiewicz, Taylor, Papadopoulos, and Onate (1990); Onate, Zienkiewicz, Surez, and Taylor (1992)]; the assumed or modified shear strain technique [Prathap (1984); Prathap (1985); Somashekar, Prathap, and Babu (1987); Bathe and Dvorkin (1985); Kim, Kim, and Lee (2004)]; and the field-consistency approach [Prathap (1984); Prathap (1985); Somashekar, Prathap, and Babu (1987)]. In these studies, where the reduced/selective integration is used, it is found that in certain cases, extra zero energy modes may exist and these techniques are not effective for thin-plate situation. The hybrid/mixed method can be considered an efficient method for avoiding shear-locking but its complex formulation and high computational cost render its usage less attractive in practical applications. The studies of the assumed/modified shear strain and the field consistency can be considered significant contributions in the development of simple bending elements in which shear locking and spurious kinematic modes have been successfully eliminated.

Several recent formulations have paralleled these developments using displacement function of the Timoshenko's beam to develop locking-free plate elements. Ibrahimbegovic (1992) and Ibrahimbegovic (1993) first used Timoshenko's beam formulas to develop three thin-thick plate elements PQ1, PQ2, PQ3 based on the mixed interpolation method. Soh, Cen and Long used a new formula similar to Timoshenko's beam formulas to present a 12-DOF quadrilateral element, ARS-Q12 [Soh, Cen, Long, and Long (2001)], and a 9-DOF triangular element, ARS-T9 [Soh, Long, and Cen (1999)]. Based on the element ARS-Q12, Cen, Long, and Yao (2002) added a bilinear in-plane displacement field of the mid-plane to build a 4-node 20-DOF quadrilateral

element CTMQ20. Some elements later were developed based on Timoshenko's beam function method such as 9-DOF triangular RDKTM [Chen and Cheung (2001)], 20-DOF quadrilateral Mindlin plate element RDKQM [Chen and Cheung (2000)], a refined 15-DOF triangular Mindlin plate element RDTMLC [Ge and Chen (2002)], a 20-DOF and 24-DOF quadrilateral element referred to as RDKQ-L20 and RDKQ-L24 [Zhang and Kim (2004)]. Because of the application of Timoshenko beam, these elements can be justified theoretically in the case of thin plates. Although these elements are efficient, they are usually used with uniform mesh. It is rather difficult to obtain accurate results when element is used in an extremely distorted geometry with challenging effects such as non-symmetric laminates which have coupling present and materials which possess a high E_1 to E_2 ratio.

To avoid problems related to element distortion encountered in finite element method (FEM), many useful techniques of mesh-free method have been recently developed [e.g. Atluri and Shen (2002); Atluri, Han, and Rajendran (2004); Mai-Duy, Khennane, and Tran-Cong (2007), etc.]. One of the best methods is the stabilized conforming nodal integration (SCNI) which is used as a normalization for nodal integration of mesh-free Galerkin weak form [Chen, Wu, and You (2001); Wang and Chen (2004); Wang, Dong, and Chen (2006)]. Although mesh-free method has good accuracy and high convergence rate, the complex approximation space increases the computational cost for numerical integrations. Recently, the application of SCNI in existing FEM for 2D elasticity problems was presented by Liu *et al.* [Liu, Dai, and Nguyen (2007); Liu, Nguyen, Dai, and Lam (2006)] as a new smoothed finite element method (SFEM). It is found that the SFEM achieves more accurate results and higher convergence rate as compared with the corresponding non-smoothed finite element method without increasing the computational cost.

The present study is a contribution to the development of a simple, accurate and locking-free four-node element, within the framework of the FSDT, which is able to work well in highly dis-

torted form for static analysis of laminated composite plates of different shapes. We will extend and develop the idea of SFEM and propose a new locking-free quadrilateral laminated plate element based on the SCNI. The present four-node 20-DOF element is obtained by incorporating the SCNI into the Bathe-Dvorkin assumed strain plate element [Bathe and Dvorkin (1985)]. The membrane and bending strain fields are approximated using strain smoothing technique of mesh-free method [Chen, Wu, and You (2001); Wang and Chen (2004)]. The shear strains are approximated by an independent interpolation field in the natural co-ordinate system. With this novel combination, the proposed element is locking free, it does not have zeros energy modes and is able to provide accurate result in cases of extremely distorted elements, for example, even when two nodes are collapsed so that the quadrilateral becomes a triangle.

The paper is outlined as follow. First, a brief review of the FSDT is introduced in section 2. The description of strain smoothing stabilization for membrane strain field, curvatures fields and the assumed natural shear strain of the element are derived in section 3. Several numerical applications are investigated in section 4 to assess the performances of the proposed element. Finally, some concluding remarks and further works are discussed in the section 5.

2 First-Order Shear Deformation Theory of Laminated Composite Plates

The first-order shear deformation theory (FSDT) is an extension of the Reissner-Mindlin theory for homogeneous isotropic thick plates. The theory take into account transverse shear strain in the formulation and it is briefly reviewed as follows [Reddy (2004)].

In FSDT, the plate kinematics is governed by the midplane displacement u_0, v_0, w_0 and the rotation θ_x, θ_y

$$\begin{aligned} u(x, y, z) &= u_0(x, y) + z\theta_x, \\ v(x, y, z) &= v_0(x, y) + z\theta_y, \\ w(x, y, z) &= w_0(x, y). \end{aligned} \quad (1)$$

A typical 4-node quadrilateral laminated plate element consisting of n layers with thickness h is shown in Figure 1.

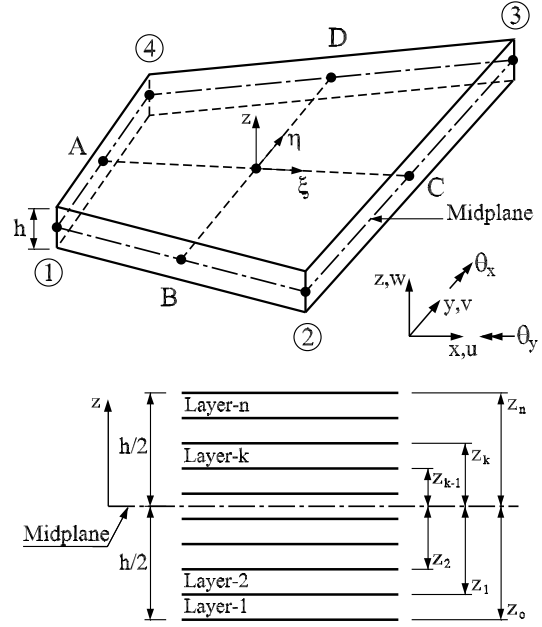


Figure 1: A quadrilateral laminated plate element consisting of n layers

The in-plane strain vector $\boldsymbol{\varepsilon} = [\varepsilon_x \ \varepsilon_y \ \varepsilon_{xy}]^T$ can be rewritten as

$$\boldsymbol{\varepsilon} = \boldsymbol{\varepsilon}_m + z\boldsymbol{\varepsilon}_b, \quad (2)$$

in which

$$\begin{aligned} \boldsymbol{\varepsilon}_m &= [u_{0,x} \ v_{0,y} \ u_{0,y} + v_{0,x}]^T; \\ \boldsymbol{\varepsilon}_b &= [\theta_{x,x} \ \theta_{y,y} \ \theta_{x,y} + \theta_{y,x}]^T, \end{aligned} \quad (3)$$

and the transverse shear strain vector $\boldsymbol{\gamma} = [\gamma_{xz} \ \gamma_{yz}]^T$ is

$$\boldsymbol{\gamma} = [\theta_x - w_{,x} \ \theta_y - w_{,y}]^T. \quad (4)$$

The stress-strain relation with respect to global x - and y -axis for the k^{th} ($k = 1..n$) lamina is expressed as

$$\begin{aligned} \boldsymbol{\sigma}^k &= \begin{Bmatrix} \sigma_x \\ \sigma_y \\ \tau_{xy} \end{Bmatrix}^k = \begin{bmatrix} \bar{Q}_{11} & \bar{Q}_{12} & \bar{Q}_{16} \\ \bar{Q}_{12} & \bar{Q}_{22} & \bar{Q}_{26} \\ \bar{Q}_{16} & \bar{Q}_{26} & \bar{Q}_{66} \end{bmatrix}^k \begin{Bmatrix} \varepsilon_x \\ \varepsilon_y \\ \gamma_{xy} \end{Bmatrix} \\ &= \bar{\mathbf{Q}}^k \boldsymbol{\varepsilon}, \end{aligned} \quad (5)$$

$$\begin{aligned} \boldsymbol{\tau}_z^k &= \begin{Bmatrix} \tau_{xz} \\ \tau_{yz} \end{Bmatrix}^k = \begin{bmatrix} k_1^2 \bar{Q}_{55}^* & k_1 k_2 \bar{Q}_{45}^* \\ k_1 k_2 \bar{Q}_{45}^* & k_2^2 \bar{Q}_{44}^* \end{bmatrix}^k \begin{Bmatrix} \gamma_{xz} \\ \gamma_{yz} \end{Bmatrix} \\ &= \bar{\mathbf{C}}_s^k \boldsymbol{\gamma}, \end{aligned} \quad (6)$$

where k_1^2, k_2^2 are SCFs and can be estimated by using special methods [Valchoutsis (1992); Chatterjee and Kulkarni (1979); Whitney (1973)] for anisotropic plates; $\bar{Q}_{ij}^k, \bar{Q}_{ij}^{*k}$ are the elastic constants of the k^{th} lamina making an angle θ^k with the principal material x -axis, which are given as

$$\bar{\mathbf{Q}}^k = \mathbf{T}_\varepsilon \mathbf{Q}^k \mathbf{T}_\varepsilon^T; \quad \bar{\mathbf{Q}}^{*k} = \mathbf{T}_\gamma \mathbf{Q}^{*k} \mathbf{T}_\gamma^T, \quad (7)$$

in which

$$\mathbf{Q}^k = \begin{bmatrix} \frac{E_1}{1-\nu_{12}\nu_{21}} & \frac{\nu_{12}E_2}{1-\nu_{12}\nu_{21}} & 0 \\ \frac{\nu_{21}E_1}{1-\nu_{12}\nu_{21}} & \frac{E_2}{1-\nu_{12}\nu_{21}} & 0 \\ 0 & 0 & G_{12} \end{bmatrix}^k, \quad (8)$$

$$\mathbf{Q}^{*k} = \begin{bmatrix} G_{13} & 0 \\ 0 & G_{23} \end{bmatrix}^k, \quad (9)$$

and $\mathbf{T}_\varepsilon, \mathbf{T}_\gamma$ are transformation matrices

$$\mathbf{T}_\varepsilon = \begin{bmatrix} c^2 & s^2 & -2cs \\ s^2 & c^2 & 2cs \\ cs & -cs & c^2 - s^2 \end{bmatrix}, \quad (10)$$

$$\mathbf{T}_\gamma = \begin{bmatrix} c & -s \\ s & c \end{bmatrix}, \quad (11)$$

where $c = \cos \theta^k, s = \sin \theta^k$.

The stress and resultant constitutive relation of the laminated plate can be expressed as

$$\boldsymbol{\sigma}_p = \begin{Bmatrix} \mathbf{N} \\ \mathbf{M} \end{Bmatrix} = \begin{bmatrix} \mathbf{A} & \mathbf{B} \\ \mathbf{B} & \mathbf{D} \end{bmatrix} \begin{Bmatrix} \boldsymbol{\varepsilon}_m \\ \boldsymbol{\varepsilon}_b \end{Bmatrix} = \mathbf{C}_p \boldsymbol{\varepsilon}_p, \quad (12)$$

$$\begin{aligned} \mathbf{T} &= \begin{Bmatrix} Q_x \\ Q_y \end{Bmatrix} = \begin{bmatrix} k_1^2 \bar{C}_{55}^\circ & k_1 k_2 \bar{C}_{45}^\circ \\ k_1 k_2 \bar{C}_{45}^\circ & k_2^2 \bar{C}_{44}^\circ \end{bmatrix} \begin{Bmatrix} \gamma_{xz} \\ \gamma_{yz} \end{Bmatrix} \\ &= \mathbf{C}_s \boldsymbol{\gamma}. \end{aligned} \quad (13)$$

where

$$\begin{aligned} A_{ij} &= \sum_{k=1}^n (z_k - z_{k-1}) \bar{Q}_{ij}^k, & i, j &= 1, 2, 6 \\ B_{ij} &= \frac{1}{2} \sum_{k=1}^n (z_k^2 - z_{k-1}^2) \bar{Q}_{ij}^k, & i, j &= 1, 2, 6 \\ D_{ij} &= \frac{1}{3} \sum_{k=1}^n (z_k^3 - z_{k-1}^3) \bar{Q}_{ij}^k, & i, j &= 1, 2, 6 \\ C_{ij}^\circ &= \sum_{k=1}^n (z_k - z_{k-1}) \bar{Q}_{ij}^{*k}, & i, j &= 4, 5 \end{aligned} \quad (14)$$

3 Strain smoothing approach for finite element method

Let us consider a bounded domain $\Omega = \sum_{i=1}^{n_e} \Omega^e$ of composite plate which is discretized into n_e finite elements. The finite element solution \mathbf{u} of a displacement model is approximated as

$$\mathbf{u} = \begin{Bmatrix} u \\ v \\ w \\ \theta_x \\ \theta_y \end{Bmatrix} = \sum_{i=1}^{np} \mathbf{N}_i \mathbf{q}_i, \quad (15)$$

where np is the total number of nodes of the mesh, \mathbf{N}_i is the shape function of the four-node serendipity element, $\mathbf{q}_i = [u_i \ v_i \ w_i \ \theta_{xi} \ \theta_{yi}]$ is the displacement vector of the element.

The corresponding approximation of membrane, bending and shear strain of equations (3) and (4) can be expressed in the following form

$$\boldsymbol{\varepsilon}_p = \begin{Bmatrix} \boldsymbol{\varepsilon}_m \\ \boldsymbol{\varepsilon}_b \end{Bmatrix} = \begin{bmatrix} \mathbf{B}_m \\ \mathbf{B}_b \end{bmatrix} \mathbf{q} = \mathbf{B}_p \mathbf{q}, \quad (16)$$

$$\boldsymbol{\gamma} = \begin{Bmatrix} \gamma_{xz} \\ \gamma_{yz} \end{Bmatrix} = \mathbf{B}_s \mathbf{q}, \quad (17)$$

$$\mathbf{B}_m = \begin{pmatrix} N_{i,x} & 0 & 0 & 0 & 0 \\ 0 & N_{i,y} & 0 & 0 & 0 \\ N_{i,y} & N_{i,x} & 0 & 0 & 0 \end{pmatrix}, \quad (18)$$

$$\mathbf{B}_b = \begin{pmatrix} 0 & 0 & 0 & N_{i,x} & 0 \\ 0 & 0 & 0 & 0 & N_{i,y} \\ 0 & 0 & 0 & N_{i,y} & N_{i,x} \end{pmatrix}, \quad (19)$$

$$\mathbf{B}_s = \begin{pmatrix} 0 & 0 & N_{i,x} & N_i & 0 \\ 0 & 0 & N_{i,y} & 0 & N_i \end{pmatrix}. \quad (20)$$

Then the element stiffness matrix can be obtained as

$$\begin{aligned} \mathbf{K}^e &= \mathbf{K}_{mb}^e + \mathbf{K}_s^e \\ &= \int_{\Omega^e} \mathbf{B}_p^T \mathbf{C}_p \mathbf{B}_p d\Omega + \int_{\Omega^e} \mathbf{B}_s^T \mathbf{C}_s \mathbf{B}_s d\Omega. \end{aligned} \quad (21)$$

In mesh-free method based on nodal integration, the convergence of the solution approximated by linear complete shape functions requires the following integration constraint (IC) to be satisfied [Chen, Wu, and You (2001); Wang and Chen

(2004)]

$$\int_{\Omega} \mathbf{B}_i^T(\mathbf{x}) d\Omega = \int_{\Gamma} \mathbf{n}^T N_i(\mathbf{x}) d\Gamma, \quad (22)$$

where \mathbf{B}_i is the standard gradient matrix associated with shape function N_i and \mathbf{n} is the matrix of outward normal to the boundary Γ .

The IC condition is met by using strain smoothing techniques for each representative nodal cell [Chen, Wu, and You (2001)]. By incorporating the idea of strain smoothing method used in mesh-free nodal integration method [Chen, Wu, and Belytschko (2000)], Liu *et al.* [Liu, Dai, and Nguyen (2007); Liu, Nguyen, Dai, and Lam (2006)] formulated the SFEM for 2D static elastic problems. The idea of formulation of SFEM is as follow: (1) elements are used as in FEM; (2) the Galerkin weak form is obtained by a mixed variational principle based on an assumed strain field and integration is carried out on the basis of element; (3) a smoothing operation is performed on each smoothing cell to normalize local strain for calculating the element stiffness matrix.

3.1 Smoothing membrane strains of the element

The membrane strains at an arbitrary point \mathbf{x}_C are obtained by using following strain smoothing operation

$$\tilde{\boldsymbol{\epsilon}}_m(\mathbf{x}_C) = \int_{\Omega_C} \boldsymbol{\epsilon}_m(\mathbf{x}) \Phi(\mathbf{x} - \mathbf{x}_C) d\Omega, \quad (23)$$

where $\boldsymbol{\epsilon}_m$ is the membrane strain obtained from displacement compatibility condition as given in Equation (16). Ω_C is the smoothing cell domain on which the smoothing operation is performed. Depending on the stability analysis [Liu, Dai, and Nguyen (2007); Liu, Nguyen, Dai, and Lam (2006)], Ω_C may be an entire element or part of an element as shown in Figure 2. Φ is a given smoothing function that satisfies at least unity property $\int_{\Omega_C} \Phi d\Omega = 1$ and is defined as

$$\Phi(\mathbf{x} - \mathbf{x}_C) = \begin{cases} 1/A_C & \mathbf{x} \in \Omega_C, \\ 0 & \mathbf{x} \notin \Omega_C. \end{cases} \quad (24)$$

where $A_C = \int_{\Omega_C} d\Omega$ is the area of the smoothing cell (subcell).

Substituting Φ into Equation (23) and applying the divergence theorem, one can get the smoothed membrane strain

$$\begin{aligned} \tilde{\boldsymbol{\epsilon}}_m(\mathbf{x}_C) &= \frac{1}{2A_C} \int_{\Omega_C} \left(\frac{\partial u_i}{\partial x_j} + \frac{\partial u_j}{\partial x_i} \right) d\Omega \\ &= \frac{1}{2A_C} \int_{\Gamma_C} (u_i n_j + u_j n_i) d\Gamma, \end{aligned} \quad (25)$$

where Γ_C is the boundary segment of the smoothing cell, Introducing the finite element approxi-

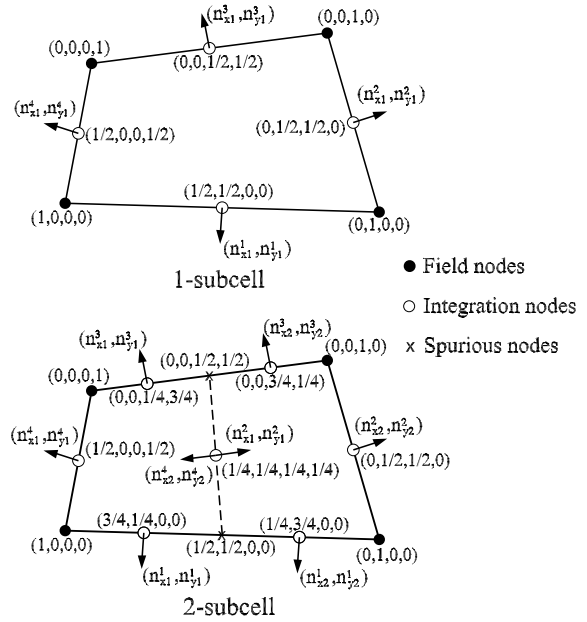


Figure 2: Subdivision of smoothing cells (nc) and the values of shape functions at nodes.

mation of u into Equation (25) gives

$$\tilde{\boldsymbol{\epsilon}}_m(\mathbf{x}_C) = \sum_{i=1}^{nc} \tilde{\mathbf{B}}_{mi}(\mathbf{x}_C) \mathbf{q}_i, \quad (26)$$

where nc is the number of smoothing cells and

$$\tilde{\mathbf{B}}_{mi}(\mathbf{x}_C) = \frac{1}{A_C} \int_{\Gamma_C} \begin{pmatrix} N_i n_x & 0 & 0 & 0 & 0 \\ 0 & N_i n_y & 0 & 0 & 0 \\ N_i n_y & N_i n_x & 0 & 0 & 0 \end{pmatrix} d\Gamma. \quad (27)$$

If one Gaussian point is used to evaluate Equation (27) along each line segment of the edge Γ_i^C of

Ω_C , Equation (27) can be transformed as follows

$$\tilde{\mathbf{B}}_{mi}(\mathbf{x}_C) = \frac{1}{A_C} \sum_{b=1}^{nb} \begin{pmatrix} N_i(\mathbf{x}_b^G)n_x & 0 & 0 & 0 & 0 \\ 0 & N_i(\mathbf{x}_b^G)n_y & 0 & 0 & 0 \\ N_i(\mathbf{x}_b^G)n_y & N_i(\mathbf{x}_b^G)n_x & 0 & 0 & 0 \end{pmatrix} l_b^C, \quad (28)$$

where \mathbf{x}_b^G and l_b^C are the midpoint (Gauss point) and the length of Γ_b^C , respectively; nb is the total number of edges of each smoothing cell.

3.2 Smoothing bending strains of the element

Similarly, by using the same constant smoothing function Φ for membrane strain, the smoothed bending strain can be obtained as follows

$$\begin{aligned} \tilde{\boldsymbol{\varepsilon}}_b(\mathbf{x}_C) &= \int_{\Omega_C} \boldsymbol{\varepsilon}_b(\mathbf{x})\Phi(\mathbf{x} - \mathbf{x}_C)d\Omega \\ &= \frac{1}{2A_C} \int_{\Gamma_C} (\theta_i n_j + \theta_j n_i) d\Gamma. \end{aligned} \quad (29)$$

Then the relationship between the smoothed bending strain field and the nodal displacement is written by

$$\tilde{\boldsymbol{\varepsilon}}_b(\mathbf{x}_C) = \sum_{i=1}^{nc} \tilde{\mathbf{B}}_{bi}(\mathbf{x}_C) \mathbf{q}_i, \quad (30)$$

with

$$\tilde{\mathbf{B}}_{bi}(\mathbf{x}_C) = \frac{1}{A_C} \int_{\Gamma_C} \begin{pmatrix} 0 & 0 & 0 & N_i n_x & 0 \\ 0 & 0 & 0 & 0 & N_i n_y \\ 0 & 0 & 0 & N_i n_y & N_i n_x \end{pmatrix} d\Gamma. \quad (31)$$

Using integration with one-point Gauss quadrature to evaluate the above equation over each line segment we get

$$\tilde{\mathbf{B}}_{bi}(\mathbf{x}_C) = \frac{1}{A_C} \sum_{b=1}^{nb} \begin{pmatrix} 0 & 0 & 0 & N_i(\mathbf{x}_b^G)n_x & 0 \\ 0 & 0 & 0 & 0 & N_i(\mathbf{x}_b^G)n_y \\ 0 & 0 & 0 & N_i(\mathbf{x}_b^G)n_y & N_i(\mathbf{x}_b^G)n_x \end{pmatrix} l_b^C. \quad (32)$$

By introducing $\tilde{\mathbf{B}}_p = [\tilde{\mathbf{B}}_m \tilde{\mathbf{B}}_b]^T$ the smoothed membrane-bending stiffness matrix of the element can be obtained by assembling the individual stiffness matrices of the smoothing cells of the

element

$$\tilde{\mathbf{K}}_{mb}^e = \sum_{C=1}^{nc} \tilde{\mathbf{B}}_{pC}^T \mathbf{C}_p \tilde{\mathbf{B}}_{pC} A_C, \quad (33)$$

where nc is the total number of smoothing cells of the element, see Figure 2.

3.3 Transverse shear strains of the element

The shear strains are approximated with independent interpolation fields in the natural coordinate system [Bathe and Dvorkin (1985)]

$$\begin{bmatrix} \gamma_\xi \\ \gamma_\eta \end{bmatrix} = \mathbf{J}^{-1} \begin{bmatrix} \gamma_\xi^A \\ \gamma_\xi^B \\ \gamma_\eta^C \\ \gamma_\eta^D \end{bmatrix}, \quad (34)$$

in which

$$\hat{\mathbf{N}} = \frac{1}{2} \begin{bmatrix} (1-\xi) & 0 & (1+\xi) & 0 \\ 0 & (1-\eta) & 0 & (1+\eta) \end{bmatrix}, \quad (35)$$

\mathbf{J} is the Jacobian matrix and the midside nodes A, B, C, D are shown in Figure 1. Expressing $\gamma_\eta^A, \gamma_\eta^C$ and $\gamma_\xi^B, \gamma_\xi^D$ in terms of the discretized fields \mathbf{u} , we obtain the shear matrix

$$\bar{\mathbf{B}}_{si} = \mathbf{J}^{-1} \begin{bmatrix} 0 & 0 & N_{i,\xi} & -b_i^{12} N_{i,\xi} & b_i^{11} N_{i,\xi} \\ 0 & 0 & N_{i,\eta} & -b_i^{22} N_{i,\eta} & b_i^{21} N_{i,\eta} \end{bmatrix}, \quad (36)$$

where

$$b_i^{11} = \xi_i x_{,\xi}^M, \quad b_i^{12} = \xi_i y_{,\xi}^M, \quad b_i^{21} = \eta_i x_{,\eta}^L, \quad b_i^{22} = \eta_i y_{,\eta}^L \quad (37)$$

in which $\xi_i \in \{-1, 1, 1, -1\}$, $\eta_i \in \{-1, -1, 1, 1\}$ and $(i, M, L) \in \{(1, B, A); (2, B, C); (3, D, C); (4, D, A)\}$.

Finally the element stiffness matrix can be obtained as follows

$$\begin{aligned} \mathbf{K}^e &= \tilde{\mathbf{K}}_{mb}^e + \bar{\mathbf{K}}_s^e \\ &= \sum_{C=1}^{nc} \tilde{\mathbf{B}}_{pC}^T \mathbf{C}_p \tilde{\mathbf{B}}_{pC} A_C + \int_{\Omega^e} \bar{\mathbf{B}}_s^T \mathbf{C}_s \bar{\mathbf{B}}_s d\Omega, \end{aligned} \quad (38)$$

where the shear term $\bar{\mathbf{K}}_s^e$ is still computed by 2×2 Gauss quadrature while the element bending stiffness $\tilde{\mathbf{K}}_{mb}^e$ in Equation (21) is replaced by

the smoothed strain technique on each smoothing cell of the element.

Once the displacement variables are known, the in-plane stresses σ_p^k for the k^{th} layer are obtained by

$$\tilde{\sigma}_p^k = \bar{Q}^k (\tilde{\epsilon}_m^o + z \tilde{\epsilon}_b^o), \quad (39)$$

and the transverse shear stresses are calculated by a simple approach of Rolfes and Rohwer (1997).

4 Numerical results and discussions

The analysis described above forms the basis of a new four-node quadrilateral element named MISQ20 (Mixed Interpolation Smoothing Quadrilateral element with 20 DOF). The 5 DOF at each node are: $u, v, w, \theta_x, \theta_y$. In this section, we will test and assess the MISQ20 element through several application studies. Two smoothing cells as shown in Figure 2 are used for calculating the smoothed membrane-bending stiffness matrix of the element. Particular plates having different shapes, boundary conditions, thickness ratios, number of layers, fibre orientations are analyzed with this element and the obtained results are discussed and compared with those obtained from other analytical and/or numerical solutions if available. The material properties considered in the numerical examples here are given in Table 1.

Table 1: Material properties.

Moduli	HM graphite epoxy			
	M1	M2	M3	M4
$E_{11} \times 10^6$	25.0	40.0	40.0	5.6
$E_{22} \times 10^6$	1.0	1.0	1.0	1.2
$G_{12} \times 10^6$	0.5	0.6	0.5	0.6
$G_{13} \times 10^6$	0.5	0.6	0.5	0.6
$G_{23} \times 10^6$	0.2	0.5	0.5	0.6
$\nu_{12} = \nu_{23} = \nu_{13}$	0.25	0.25	0.25	0.26

4.1 Example 1: Simply supported cross-ply laminates under uniformly distributed load

The symmetric $[0^\circ/90^\circ/0^\circ]$ and unsymmetric $[0^\circ/90^\circ]$ cross-ply laminate square plates of ma-

terial M1 with length a and thickness h , subjected to simply supported boundary SS1 [Reddy (2004)] under a uniform transverse load $q_o = 1$ are studied. The shear correction factors are constant and equal to 5/6.

Owing to symmetry, only a quarter of the plate is discretized using 3×3 , 6×6 , 12×12 meshes with regular as well as highly distorted elements as shown in Figure 3. Table 2 shows the

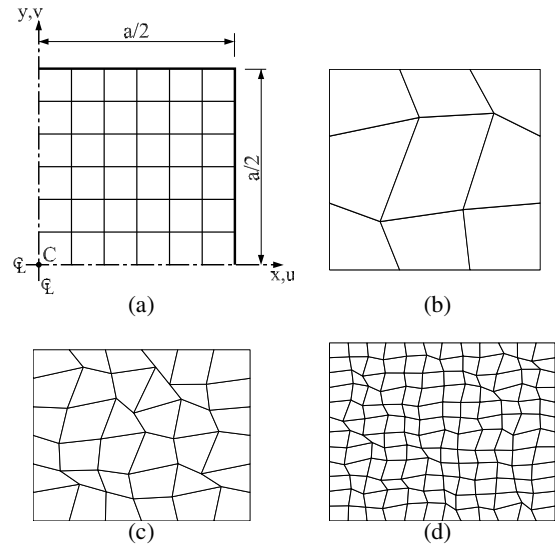


Figure 3: Example 1. Meshes of a quarter of simply supported plate: (a) typical regular mesh 6×6 ; (b) irregular mesh 3×3 ; (c) irregular mesh 6×6 ; (d) irregular mesh 12×12

prediction accuracies and convergence rate for the dimensionless plate center deflections $w = 100E_2wh^3/(q_oa^4)$ with two types of meshes. It is found that the accuracy of the present element is better than EML4 (Enhance Mixed Linked 4 node) element [Auricchio and Sacco (1999)], HASL (Hybrid Assumed-Strain Laminate) element [Cazzani, Garusi, Tralli, and Atluri (2005)] in the case of regular meshes 12×12 . Numerical results in Table 2 also indicate that element performance, in terms of rate of convergence and accuracy, with respect to exact solution is excellent. It is interesting to note that the proposed MISQ20 yields not only accurate results in a wide range of thick to thin plates but also rapid convergence, especially when plates are thin for both regular

Table 2: Example 1. Simply supported cross-ply $[0^\circ/90^\circ]$ and $[0^\circ/90^\circ/0^\circ]$ square plate under uniform load: Convergence of normalized central deflection $w^* = 100E_2wh^3/(q_0a^4)$ and comparison with available literature.

h/a	Lay-up	Mesh	EML4 12×12	HASL 12×12	MISQ20			Exact
					3×3	6×6	12×12	
0.001		Regular	–	–	1.6897	1.6943	1.6952	–
		Irregular	–	–	1.6813	1.6918	1.6947	–
0.01	$[0^\circ/90^\circ]$	Regular	–	–	1.6923	1.6967	1.6979	1.6980
		Irregular	–	–	1.6862	1.6928	1.6973	–
0.1		Regular	1.9470	–	1.9465	1.9469	1.9469	1.9468
		Irregular	–	–	1.9516	1.9478	1.9466	–
0.001		Regular	–	–	0.6736	0.6676	0.6664	–
		Irregular	–	–	0.6728	0.6676	0.6667	–
0.01	$[0^\circ/90^\circ/0^\circ]$	Regular	–	0.6700	0.6773	0.6713	0.6700	0.6697
		Irregular	–	–	0.7006	0.6736	0.6702	–
0.1		Regular	1.0220	1.0262	1.0367	1.0254	1.0227	1.0219
		Irregular	–	–	1.0735	1.0312	1.0232	–

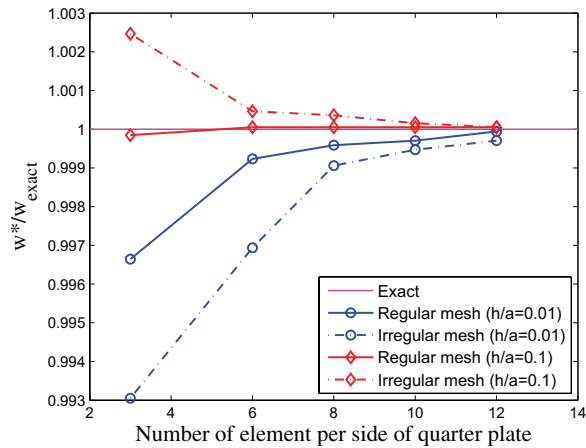
Table 3: Example 2. Simply supported 2-layer angle-ply $[\theta/ - \theta]$ square plate under uniform load: Convergence of the normalized central deflection $w^* = 100E_2wh^3/(q_0a^4)$ with different fibre angles and comparison with available literature.

Fibre angle	Exact	MQH3T	SQUAD4	RDTMLC	RDKQ-L20	MISQ20			
		6×6 (665DOF)	10×10 (605DOF)	8×8 (605DOF)	10×10 (605DOF)	4×4	6×6	8×8	10×10 (605DOF)
$\pm 5^\circ$	0.4736	0.4764	0.4776	0.4776	0.4742	0.4987	0.4793	0.4758	0.4748
$\pm 15^\circ$	0.7142	0.7160	–	0.7014	0.7139	0.7328	0.7191	0.7164	0.7155
$\pm 25^\circ$	0.7870	0.7870	0.8030	0.7638	0.7854	0.7980	0.7901	0.7886	0.7880
$\pm 35^\circ$	0.7561	0.7555	0.7745	0.7329	0.7538	0.7633	0.7581	0.7571	0.7567
$\pm 45^\circ$	0.7322	0.7315	0.7506	0.7106	0.7302	0.7381	0.7340	0.7331	0.7327

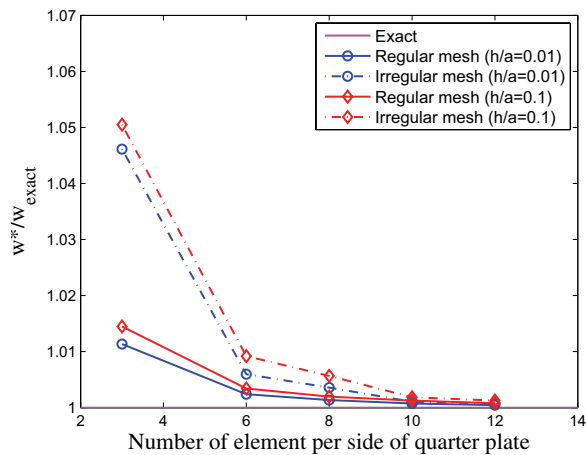
Table 4: Example 3. Clamped 2-layer angle-ply $[\theta/ - \theta]$ square plate under uniform load: Convergence of normalized central deflection $w^* = 100E_2wh^3/(q_0a^4)$ with different fibre angles and comparison with available literature.

Fibre angle	Exact	MQH3T	SQUAD4	RDTMLC	RDKQ-L20	MISQ20			
		6×6 (665DOF)	10×10 (605DOF)	8×8 (605DOF)	10×10 (605DOF)	4×4	6×6	8×8	10×10 (605DOF)
$\pm 5^\circ$	0.0946	0.1083	0.1040	0.1095	0.1046	0.1143	0.1010	0.1013	0.1023
$\pm 15^\circ$	0.1691	0.2009	–	0.1944	0.1990	0.2096	0.1961	0.1964	0.1971
$\pm 25^\circ$	0.2355	0.2572	0.2602	0.2466	0.2600	0.2723	0.2578	0.2579	0.2580
$\pm 35^\circ$	0.2763	0.2844	0.2914	0.2726	0.2908	0.3073	0.2909	0.2895	0.2889
$\pm 45^\circ$	0.2890	0.2929	0.3013	0.2809	0.3004	0.3181	0.3013	0.2993	0.2986

and extremely distorted meshes. The effect of distorted mesh and decreasing thickness ratio h/a on the convergence of the results is shown in Figure 4. It is found that the convergence solution of w for unsymmetric cross-ply $[0^\circ/90^\circ]$ with $h/a = 0.1$ is faster than $h/a = 0.01$ in both types of mesh. For symmetric cross-ply $[0^\circ/90^\circ/0^\circ]$, the convergence rate of w^* with $h/a = 0.1$ is slower than with $h/a = 0.01$.



(a) $(0^\circ/90^\circ)$



(b) $(0^\circ/90^\circ/0^\circ)$

Figure 4: Example 1. Convergence behaviour of the normalized central deflection w^* .

4.2 Example 2: Simply supported angle-ply square plate under uniformly distributed load

A simply supported two-layer angle-ply $[\theta^\circ / -\theta^\circ]$ square plate of material M3 with length $a =$

10 and thickness $h = 0.02$, subjected to a uniformly distributed transverse load $q_o = 1$ is analyzed. Shear correction factors are: $k_1^2 = k_2^2 = 5/6$. The total thickness of θ° and $-\theta^\circ$ layers are equal. Due to asymmetry, the entire plate is modelled using $4 \times 4, 6 \times 6, 8 \times 8, 10 \times 10$ meshes. A representative sketch of the 6×6 mesh used in this analysis is shown in Figure 5.

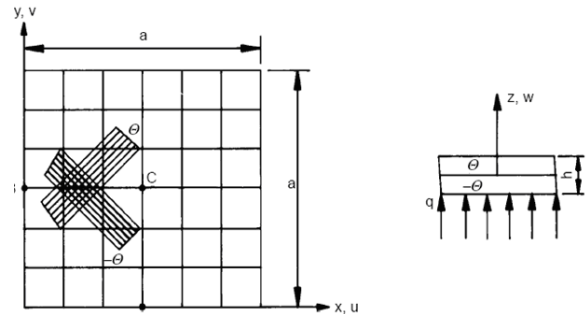


Figure 5: Example 2. Finite element and geometry data for unsymmetric angle-ply plate.

Table 3 presents a convergence study of the normalized central deflection $w^* = 100E_2wh^3/(q_oa^4)$ for the simply supported two-layer square plate with different fibre orientation angles. The normalized central deflection w^* is compared with the numerical solutions obtained using MQH3T [Spilker, Jakobs, and Engelmann (1985)] (hybrid laminated element), SQUAD4 [Wilt, Saleeb, and Chang (1990)] (mixed laminated element), RDTMLC [Ge and Chen (2002)] (refined discrete triangular laminated element), RDKQ-L20 [Zhang and Kim (2004)] (refined discrete quadrilateral laminate element) and the exact solution given by Whitney [Whitney (1969); Whitney (1970)]. The effect of fibre orientation on the accuracy of the methods is also shown in Figure 6.

From Table 3 and Figure 6, it can be seen that the accuracy of the present element compares very favorably with other elements and the method is convergent with mesh refinement as shown in Table 3. The accuracy obtained with the present MISQ20 element is quite insensitive with fibre an-

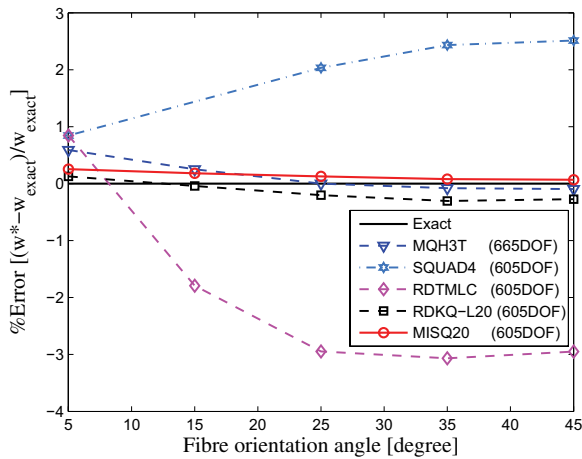


Figure 6: Example 2. The effect of θ on the accuracy of w^* .

gles while other methods behave badly in some cases as shown in Figure 6 and Table 3.

4.3 Example 3: Clamped angle-ply square plate under uniformly distributed load

The same plate as in example 2 (section 4.2) is analyzed here except that all the plate edges are clamped. The obtained numerical results of the normalized central deflection $w^* = 100E_2wh^3/(q_0a^4)$ is shown in Table 4. The effect of fibre orientation on the accuracy of different methods is also shown in Figure 7.

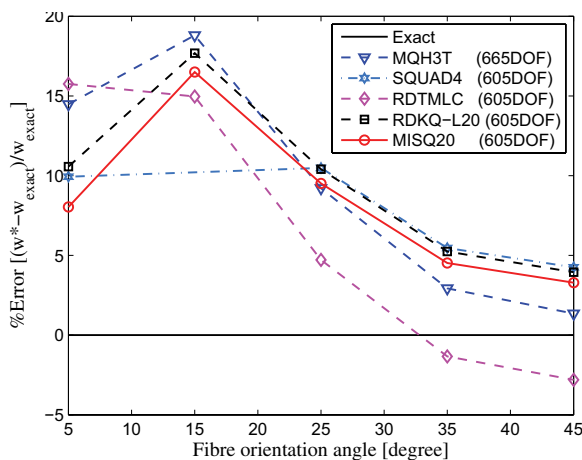


Figure 7: Example 3. The effect of θ on the accuracy of w^* .

From Table 4, it is evident that with an 8×8 mesh for the whole plate, the present element gives more accurate results than the SQUAD4 element with a 10×10 mesh and the RDKQ-L20 element with a 10×10 mesh. The present results with a 10×10 mesh are comparable to those of MQH3T with a 6×6 mesh and RDTMLC with an 8×8 mesh but the degrees of freedom associated with MQH3T elements are much larger (665 DOF compared with 605 DOF).

4.4 Example 4: Antisymmetric angle-ply 2-layer $[-45^\circ/45^\circ]$ and 8-layer $[-45^\circ/45^\circ]_4$ square plate with simply supported edges under a double sinusoidal load

To study the combined effect of bending-inplane shear, extension twist coupling caused by B_{16} and B_{26} in Equation (12) and transverse shear flexibility on the performance of the proposed element, simply-supported 2-layer $[-45^\circ/45^\circ]$ and 8-layer $[-45^\circ/45^\circ]_4$ angle-ply square plates, with length a and thickness h subjected to doubly sinusoidal loading $q = q_0 \sin(x/a) \sin(y/a)$ as shown in Figure 8, are analyzed. The SCFs for the plate made of material M3 are assumed 5/6.

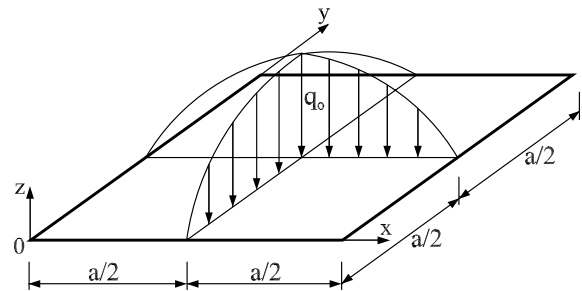


Figure 8: Example 4. Geometry data for unsymmetric angle-ply square plate.

Due to anti-symmetry, the whole plate is modeled with 10×10 meshes. The numerical results shown in Table 5 demonstrate the accuracy of the present method. Note that calculations are performed for the normalized central deflection $w^* = 1000E_2wh^3/(q_0a^4)$; the normalized stress $\sigma_x^* = \sigma_x h^2/(q_0a^2)$ at point $(a/2, a/2, h/2)$; the shear stress $\tau_{xy}^* = \tau_{xy} h^2/(q_0a^2)$ at point $(0, 0, -h/2)$

Table 5: Example 4. Simply supported 2-layer $[-45^\circ/45^\circ]$ and 8-layer $[-45^\circ/45^\circ]_4$ angle-ply square plate under doubly sinusoidal loading: Comparison of normalized central deflection and normalized stresses. Note that σ_x^* is computed at point $(a/2, a/2, h/2)$; τ_{xy}^* at point $(0, 0, -h/2)$ and τ_{xz}^* at point $(0, a/2, h/4)$.

h/a	Model	$[-45^\circ/45^\circ]$				$[-45^\circ/45^\circ]_4$			
		w^*	σ_x^*	τ_{xy}^*	τ_{xz}^*	w^*	σ_x^*	τ_{xy}^*	τ_{xz}^*
0.01	CTMQ20 (8×8)	0.6519	0.2474	0.2295	0.1194	0.2463	0.1459	0.1356	0.1791
	RDKQ-L20 (10×10)	0.6533	0.2488	0.2302	0.1245	0.2466	0.1464	0.1359	0.1813
	MFE (8×8)	0.6558	–	–	–	0.2472	–	–	–
	MISQ20 (10×10)	0.6553	0.2459	0.2304	0.1884	0.2475	0.1427	0.1368	0.2358
	Exact (FSDT)	0.6564	0.2498	0.2336	0.2143	0.2479	0.1384	0.1384	0.2487
0.1	CTMQ20 (8×8)	0.8218	0.2543	0.2349	0.2005	0.4157	0.1507	0.1361	0.2384
	RDKQ-L20 (10×10)	0.8241	0.2517	0.2316	0.2053	0.4171	0.1512	0.1370	0.2420
	MFE (8×8)	0.8257	–	–	–	0.4189	–	–	–
	MISQ20 (10×10)	0.8286	0.2459	0.2304	0.1884	0.4208	0.1427	0.1368	0.2358
	Exact (FSDT)	0.8284	0.2498	0.2336	0.2143	0.4198	0.1445	0.1384	0.2487

Table 6: Example 5. Clamped 9-layer $[(0^\circ/90^\circ)_2/0]_s$ cross-ply square plate under uniform load: Comparison of normalized central deflection $w^* = 1000E_2wh^3/(q_0a^4)$.

h/a	QUAD4 8×8 (405DOF)	TRIPLT 4×4 (375DOF)	MFE 8×8 (486DOF)	RDTML 10×10 (605DOF)	RDKQ-L20 5×5 (180DOF)	MISQ20 5×5 (180DOF)	SQH
0.0001	0.944	–	–	0.957	0.969	0.940	–
0.001	0.944	0.934	0.949	0.957	0.969	0.940	0.949
0.01	0.957	0.964	0.963	0.969	0.983	0.955	0.963
0.1	2.316	2.320	2.331	2.318	2.351	2.341	2.319

and the normalized transverse shear stress $\tau_{xz}^* = \tau_{xz}h/(q_0a)$ at point $(0, a/2, h/4)$.

4.5 Example 5: Clamped 9-layer $[(0^\circ/90^\circ)_2/0]_s$ cross-ply square plate under uniformly distributed load

A clamped 9-layered symmetrically laminated cross-ply $[(0^\circ/90^\circ)_2/0]_s$ plate of length a and thickness h under uniform load q_0 is considered. The SCFs are: $k_1^2 = 1.054$ and $k_2^2 = 0.917$ [Zhang and Kim (2004)]. The total thicknesses of 0° and 90° layers of material M1 are the same. This particular lay-up is known as especially orthotropic as it does not exhibit any coupling. Making use of this feature, only one quarter of the plate is discretized. The normalized central deflection $w^* = 1000E_2wh^3/(q_0a^4)$ of the clamped square plate with various aspect ratios h/a is calculated with a 5×5 mesh, and the results are compared

in Table 6 with those from QUAD4 [Somashekar, Prathap, and Babu (1987)] with an 8×8 mesh, TRIPLT [Pagano (1970)] with a 4×4 mesh MFE [Singh, Raveendranath, and Rao (2000)] with an 8×8 mesh, RDTMLC [Ge and Chen (2002)] with a 10×10 mesh, RDKQ-L20 [Zhang and Kim (2004)] with a 5×5 mesh and exact solution from FSDT [Reddy (2004)].

Table 7: Example 5. Clamped 9-layer $[(0^\circ/90^\circ)_2/0]_s$ cross-ply square plate under uniform load: Comparison of normalized central moment resultant $M_x^* = 100E_2M_x/(q_0a^2)$.

h/a	QUAD4	TRIPLT	MFE	MISQ20
0.01	-6.61	-6.62	-6.58	-6.50
0.1	-5.66	-5.66	-5.59	-5.57

The comparison of normalized central moment

$M_x^* = 100E_2M_x/(q_0a^2)$ is also presented in Table 7.

4.6 Example 6: Simply supported 9-layer $[(0^\circ/90^\circ)_2/0]_s$ cross-ply square plate under uniformly distributed load

To assess the effect of boundary conditions on MISQ20 element, the plate in the previous example 5 is re-analyzed with simply supported boundaries. The results are listed in Table 8 and Table 9 which show that the present results are accurate and comparable with those obtained with other elements. The present element can provide accurate prediction of the solution with much reduced degrees of freedom in some cases.

Table 8: Example 6. Simply supported 9-layer $[(0^\circ/90^\circ)_2/0]_s$ cross-ply square plate under uniform load: Comparison of normalized central moment resultant $M_x^* = 1000E_2M_x/(q_0a^2)$.

h/a	QUAD4	TRIPLT	MFE	MISQ20	Exact
0.001	8.88	8.42	8.90	9.02	8.89
0.01	8.88	8.81	8.90	9.02	8.88
0.1	8.84	8.42	8.44	8.80	8.42

4.7 Example 7: A clamped circular plate subjected to uniform pressure

A clamped circular plate of material M4 with radius R and various aspect ratios of R/h subjected to uniformly distributed load is considered. The laminate is unidirectional with fibers oriented at $\theta = 0^\circ$ with respect to the global coordinates. The SCFs are $5/6$. Owing to symmetry, only a quarter of the circular plate is modelled with 12 and 48 elements as shown in Figure 9. The results are compared with numerical results of the SQUAD4 element [Wilt, Saleeb, and Chang (1990)], the RDKQ-L20 element [Zhang and Kim (2004)], RDTMLC element [Ge and Chen (2002)] and the exact solution [Reddy (2004)] in Table 10. Note that the normalized central deflection of the circular plate in Table 10 is $w^* = wD/(qR^4)$ with $D = 3(D_{11} + D_{22}) + 2(D_{12} + 2D_{66})$, where $D_{11}, D_{22}, D_{12}, D_{66}$

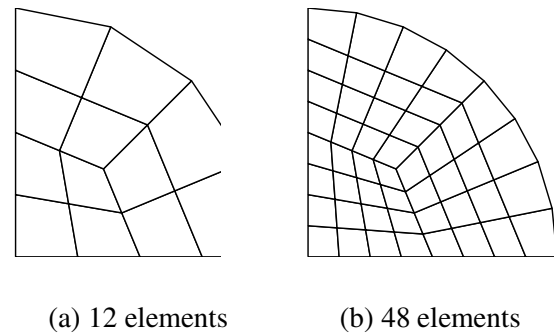


Figure 9: Example 7. Finite element meshes of a quarter of circular plate.

are bending rigidity coefficients of the laminate found by laminate theory.

From the data of Table 10, it can be seen that the present elements give more accurate solution for both thick and thin plate than those of cited elements.

4.8 Example 8: Simply supported cross-ply $[0^\circ/90^\circ/0^\circ]$ and angle-ply $[45^\circ/-45^\circ/45^\circ]$ skew laminated plates under uniformly distributed load

This section deals with symmetric cross-ply $[0^\circ/90^\circ/0^\circ]$ and angle-ply $[45^\circ/-45^\circ/45^\circ]$ skew laminated plates of material M1 with length $a = 10$ and thickness $h = 0.1$, subjected to simply supported boundary under a uniform load as shown in Figure 10. The SCFs are equal to $5/6$. The skew angle α is varied from 0° to 45° . The entire plate is modelled using 8×8 , 10×10 and 12×12 meshes. A representative example of the 10×10 mesh used in this analysis is shown in Figure 10.

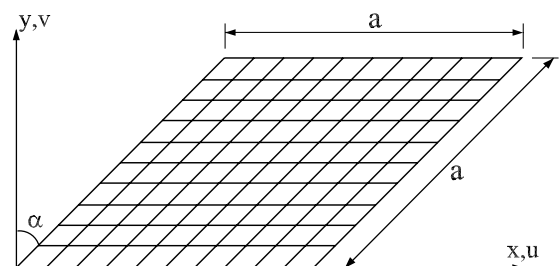


Figure 10: Example 8. Finite element and geometry data of skew plate.

Table 9: Example 6. Simply supported 9-layer $[(0^\circ/90^\circ)_2/0]_s$ cross-ply square plate under uniform load: Comparison of normalized central deflection $w^* = 1000E_2wh^3/(q_0a^4)$.

h/a	QUAD4 8×8 (405DOF)	TRIPLT 4×4 (375DOF)	MFE 8×8 (486DOF)	RDTML 10×10 (605DOF)	RDKQ-L20 5×5 (180DOF)	MISQ20 5×5 (180DOF)	Exact
0.0001	4.46	–	–	4.470	4.475	4.467	4.47
0.001	4.46	4.45	4.47	4.471	4.475	4.467	4.47
0.01	4.47	4.48	4.49	4.483	4.488	4.481	4.49
0.1	5.84	5.85	5.86	5.858	5.851	5.864	5.85

Table 10: Example 7. Clamped circular plate under uniform loading: Comparison of normalized central deflection $w^* = wD/(qR^4)$.

R/h	RDTMLC	SQUAD4	RDKQ-L20		MISQ20		Exact
	96	48	12	48	12	48	
1000	0.1265	0.1231	0.1269	0.1259	0.1271	0.1258	0.1250
100	0.1266	0.1242	0.1245	0.1251	0.1273	0.1259	–
50	0.1268	0.1247	0.1244	0.1251	0.1277	0.1264	–
25	0.1276	0.1264	0.1244	0.1251	0.1293	0.1280	–
16.67	0.1291	0.1291	0.1244	0.1251	0.1320	0.1308	–
10	0.1344	0.1378	0.1244	0.1251	0.1407	0.1394	–

Since very few results are available for static analysis of skew composite plates, the present results are only compared with some results of Chakrabarti, Sengupta, and Sheikh (2004) based on FSDT and higher order shear deformation theory (HSDT) as given in the Table 11. The present results in general indicate a good agreement. However, it can be observed that the deflection and stress are closer to those of HSDT than FSDT.

4.9 Example 9: A clamped triangular plate subjected to uniform pressure

The last problem considered in this section is that of a triangular plate, clamped on all sides subjected to a uniform load q_0 . The unidirectional laminate of material M4 is investigated with the fibres oriented at an angle $\theta = 0^\circ$ with respect to global x -axis. The reference solution is taken from Wilt, Saleeb, and Chang (1990) and a typical mesh of 48 elements as shown in Figure 11 was chosen on the basis of results from SQUAD4 element [Wilt, Saleeb, and Chang (1990)].

The deflections $w^* = 1000E_2wh^3/(q_0a^4)$ for various plate aspect ratios are given in Table 12. As

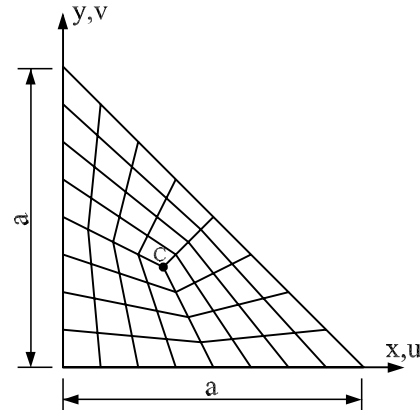


Figure 11: Example 9. Finite element and geometry data for triangle plate.

shown, the discrepancy between the present and SQUAD4 results decreases when the h/a ratio decreases, except for the case $h/a = 0.001$. However, in all cases of the thickness to span h/a ratio, the difference between the two results is always lower than 4%.

Table 11: Example 8. Simply supported skew plate: Comparison of normalized central deflection and stress.

α	Model	[0°/90°/0°]		[45°/-45°/45°]	
		$w^*(a/2, a/2, 0)$	$\sigma_x^*(a/2, a/2, h/2)$	$w^*(a/2, a/2, 0)$	$\sigma_x^*(a/2, a/2, h/2)$
0°	MISQ20 (8×8)	6.7365	0.7846	5.9825	0.2770
	MISQ20 (10×10)	6.7219	0.7930	6.0128	0.2766
	MISQ20 (12×12)	6.7146	0.7975	6.0397	0.2771
	HSDT (16×16)	6.7222	0.8211	5.9502	0.2739
	FSDT (16×16)	6.7090	0.8159	5.9515	0.2743
15°	MISQ20 (8×8)	6.4526	0.7493	6.4700	0.2559
	MISQ20 (10×10)	6.4417	0.7587	6.4873	0.2622
	MISQ20 (12×12)	6.4367	0.7634	6.5027	0.2656
	HSDT (16×16)	6.4437	0.7858	6.4391	0.2692
	FSDT (16×16)	6.4321	0.7812	6.4332	0.2693
30°	MISQ20 (8×8)	5.4708	0.6321	5.8039	0.2511
	MISQ20 (10×10)	5.4681	0.6424	5.8150	0.2563
	MISQ20 (12×12)	5.4687	0.6476	5.8234	0.2593
	HSDT (16×16)	5.4732	0.6664	5.7955	0.2658
	FSDT (16×16)	5.4654	0.6634	5.7904	0.2651
45°	MISQ20 (8×8)	3.6305	0.4208	3.5984	0.2210
	MISQ20 (10×10)	3.6333	0.4326	3.6149	0.2251
	MISQ20 (12×12)	3.6396	0.4387	3.6275	0.2270
	HSDT (16×16)	3.6323	0.4516	3.6324	0.2329
	FSDT (16×16)	3.6300	0.4505	3.6301	0.2323

Table 12: Example 9. Clamped triangular plate under uniform load: Comparison of normalized centroidal deflection $w^* = 1000E_2wh^3/(q_0a^4)$.

h/a	SQUAD4	MISQ20	%Error
0.001	0.9452	0.9795	3.629
0.01	0.9975	0.9890	-0.852
0.02	1.0406	1.0174	-2.229
0.04	1.1641	1.1289	-3.024
0.06	1.3517	1.3085	-3.196
0.1	1.9200	1.8515	-3.568

5 Concluding remarks

An accurate simple four-node 20-DOF displacement-based quadrilateral element MISQ20 has been developed and reported in this paper for linear analysis of thin to thick laminated plates of various shapes. The element is based on mixed interpolation with strain smoothing

technique used in Galerkin mesh-free method and it is easy to implement. With this combination, the element maintains a sufficient rank and free from shear locking and any spurious modes. Several numerical examples are studied and the obtained results are in excellent agreement with analytical solution. It is found that the new proposed element is fully robust, reliable and is not sensitive to mesh distortion. It can yield accurate result even with coarse discretization irrespective of the thickness ratio and stacking sequence.

Although only plate bending problems are considered in this work, there is no difficulty to extend this element to other problems such as dynamic analysis, geometric nonlinear analysis of laminated plates/shells or elasto-plastic nonlinear problems. All of these perspectives will be shown in further papers.

Acknowledgement: The first author is sup-

ported by the Faculty of Engineering and Surveying (FoES) and the Computational Engineering & Science Research Center (CESRC), USQ, Australia. These supports are gratefully acknowledged.

References

- Atluri, S. N.; Han, Z. D.; Rajendran, A. M.** (2004): A new implementation of the meshless finite volume method, through the MLPG "mixed" approach. *CMES: Computer Modeling in Engineering & Sciences*, vol. 6, pp. 491–514.
- Atluri, S. N.; Shen, S. P.** (2002): *The meshless local Petrov-Galerkin (MLPG) method*. Tech. Science Press.
- Auricchio, F.; Sacco, E.** (1999): A mixed-enhanced finite-element for the analysis of laminated composite plates. *International Journal for Numerical Methods in Engineering*, vol. 44, pp. 1481–1504.
- Bathe, K.; Dvorkin, E.** (1985): A four node plate bending element based on Mindlin-Reissner plate theory and a mixed interpolation. *International Journal for Numerical Methods in Engineering*, vol. 21, pp. 367–383.
- Cazzani, A.; Garusi, E.; Tralli, A.; Atluri, S.** (2005): A four-node hybrid assumed-strain finite element for laminated composite plate. *CMC: Computers, Materials & Continua*, vol. 2, pp. 23–38.
- Cen, S.; Long, Y. Q.; Yao, Z. H.** (2002): A new hybrid-enhanced displacement-based element for the analysis of laminated composite plates. *Computers and Structures*, vol. 80, pp. 819–833.
- Chakrabarti, A.; Sengupta, S.; Sheikh, A.** (2004): Analysis of skew composite plates using a new triangular element based on higher order shear deformation theory. *IE(I) Journal-CV*, vol. 85, pp. 77–83.
- Chatterjee, S.; Kulkarni, S.** (1979): Shear correction factors for laminated plates. *AIAA Journal*, vol. 17, pp. 498–499.
- Chen, J.; Wu, C.; Belytschko, T.** (2000): Regularization of material instabilities by meshfree approximations with intrinsic length scales. *International Journal for Numerical Methods in Engineering*, vol. 47, pp. 1303–1322.
- Chen, J.; Wu, C.; You, Y.** (2001): A stabilized conforming nodal integration for Galerkin meshfree method. *International Journal for Numerical Methods in Engineering*, vol. 50, pp. 435–466.
- Chen, W.; Cheung, Y.** (2000): Refined quadrilateral element based on Mindlin/Reissner plate theory. *International Journal for Numerical Methods in Engineering*, vol. 47, pp. 605–627.
- Chen, W.; Cheung, Y.** (2001): Refined 9-Dof triangular Mindlin plate elements. *International Journal for Numerical Methods in Engineering*, vol. 51, pp. 1259–1281.
- Crisfield, M.** (1984): A quadratic Mindlin element using shear constraints. *Computers and Structures*, vol. 18, pp. 833–852.
- Ge, Z.; Chen, W.** (2002): A refined discrete triangular Mindlin element for laminated composite plates. *Structural Engineering and Mechanics*, vol. 14, pp. 575–593.
- Hughes, T.; Cohen, M.; Haroun** (1978): Reduced and selective integration techniques in finite element analysis of plates. *Nuclear Engineering Design*, vol. 46, pp. 203–222.
- Hughes, T.; Tezduar, T.** (1981): Finite elements based upon Mindlin plate theory with particular reference to the four-node bilinear isoparametric element. *Journal of Applied Mechanics*, vol. 48, pp. 587–596.
- Ibrahimbegovic, A.** (1992): Plate quadrilateral finite elements with incompatible modes. *Communications in Applied Numerical Methods*, vol. 8, pp. 497–504.
- Ibrahimbegovic, A.** (1993): Quadrilateral finite elements for analysis of thick in thin plates. *Computer Methods in Applied Mechanics and Engineering*, vol. 110, pp. 195–209.

- Kim, J.; Kim, Y. H.; Lee, S. W.** (2004): Asymptotic Postbuckling Analysis of Composite and Sandwich Structures via the Assumed Strain Solid Shell Element Formulation. *CMES: Computer Modeling in Engineering & Science*, vol. 6, no. 2, pp. 121–144.
- Liu, G.; Dai, K.; Nguyen, T.** (2007): A smoothed finite element method for mechanics problems. *Computational Mechanics*, vol. 39, no. 6, pp. 859–877.
- Liu, G.; Nguyen, T.; Dai, K.; Lam, K.** (2006): Theoretical aspects of the smoothed finite element method (SFEM). *International Journal for Numerical Methods in Engineering*, vol. (in press).
- Mai-Duy, N.; Khennane, A.; Tran-Cong, T.** (2007): Computation of laminated composite plates using integrated radial basis function networks. *CMC: Computers, Materials & Continua*, vol. 5, pp. 63–77.
- Malkus, D.; Hughes, T.** (1978): Mixed finite element methods-reduced and selective integration techniques: a unification of concepts. *Computer Methods in Applied Mechanics and Engineering*, vol. 15, pp. 63–81.
- Onate, E.; Zienkiewicz, O.; Surez, B.; Taylor, T.** (1992): A general methodology for deriving shear constrained Reissner-Mindlin plate elements. *International Journal for Numerical Methods in Engineering*, vol. 33, pp. 345–367.
- Pagano, N.** (1970): Exact solutions for rectangular bi-directional composites and sandwich plates. *Journal of Composite Materials*, vol. 4, pp. 20–34.
- Pawsey, S.; Clough, R.** (1971): Improved numerical integration of thick shell finite elements. *International Journal for Numerical Methods in Engineering*, vol. 3, pp. 575–586.
- Prathap, G.** (1984): An optimally constrained 4-noded quadrilateral thin plate bending element. *Computers and Structures*, vol. 18, pp. 789–794.
- Prathap, G.** (1985): A C0 continuous 4-noded cylindrical shell element. *Computers and Structures*, vol. 21, pp. 995–999.
- Pugh, E.; Hinton, E.; Zienkiewicz, O.** (1978): A study of quadrilateral plate bending elements with reduced integration. *International Journal for Numerical Methods in Engineering*, vol. 12, pp. 1059–1079.
- Reddy, J.** (2004): *Mechanics of laminated composite plates and shells-Theory and analysis*. CRC Press.
- Rolfes, R.; Rohwer, K.** (1997): Improved transverse shear stresses in composite finite elements based on first order shear deformation theory. *International Journal for Numerical Methods in Engineering*, vol. 40, pp. 51–60.
- Singh, G.; Raveendranath, P.; Rao, G. V.** (2000): An accurate four-node shear flexible composite plate element. *International Journal for Numerical Methods in Engineering*, vol. 47, pp. 1605–1620.
- Soh, A.; Cen, S.; Long, Y.; Long, Z.** (2001): A new twelve DOF quadrilateral element for analysis of thick and thin plates. *European Journal of Mechanics - A/Solids*, vol. 20, pp. 299–326.
- Soh, A.; Long, Z.; Cen, S.** (1999): A new nine d.o.f triangular element for analysis of thick and thin plates. *Computers and Mechanics*, vol. 24, pp. 408–417.
- Somashekar, B.; Prathap, G.; Babu, R.** (1987): A field consistent four-noded laminated anisotropic plate/shell element. *Computers and Structures*, vol. 25, pp. 345–353.
- Spilker, R.; Jakobs, D.; Engelmann, B.** (1985): Efficient hybrid stress isoparametric elements for moderately thick and thin multiplayer plates. *Hybrid and Mixed Finite Element Method*, vol. 73, pp. 113–122.
- Valchoutsis, S.** (1992): Shear correction factors for plates and shells. *International Journal for Numerical Methods in Engineering*, vol. 33, pp. 1537–1552.
- Wang, D.; Chen, J.** (2004): Locking-free stabilized conforming nodal integration for meshfree Mindlin-Reissner plate formulation. *Computer*

Methods in Applied Mechanics and Engineering, vol. 193, pp. 1065–1083.

Wang, D.; Dong, S. B.; Chen, J. (2006): Extended meshfree analysis of transverse and in-plane loading of a laminated anisotropic plate of general planform geometry. *International Journal of Solids and Structures*, vol. 43, pp. 144–171.

Whitney, J. (1969): Bending-extensional coupling in laminated plates under transverse load. *Journal of Composite Materials*, vol. 3, pp. 398–411.

Whitney, J. (1970): The effect of boundary conditions on the response of laminated composites. *Journal of Composite Materials*, vol. 4, pp. 192–203.

Whitney, J. (1973): Shear correction factors for orthotropic laminates under static load. *Journal of Applied Mechanics*, vol. 40, pp. 302–304.

Wilt, T.; Saleeb, A.; Chang, T. (1990): Mixed element for laminated plates and shells. *Computers and Structures*, vol. 37, pp. 597–611.

Zhang, Y. X.; Kim, K. S. (2004): Two simple and efficient displacement-based quadrilateral elements for the analysis of the composite laminated plates. *International Journal for Numerical Methods in Engineering*, vol. 61, pp. 1771–1796.

Zienkiewicz, O.; Taylor, R.; Papadopoulos, P.; Onate, E. (1990): Plate bending elements with discrete constraints: new triangular elements. *Computers and Structures*, vol. 35, pp. 505–522.

Zienkiewicz, O. C.; Taylor, R.; Too, J. (1971): Reduced integration technique in general analysis of plates and shells. *International Journal for Numerical Methods in Engineering*, vol. 3, pp. 275–290.

